JOURNAL OF BACTERIOLOGY, Jan. 2007, p. 109–118 Vol. 189, No. 1
0021-9193/07/$08.00+0 doi:10.1128/JB.00710-06

Pirin Regulates Pyruvate Catabolism by Interacting with the Pyruvate Dehydrogenase E1 Subunit and Modulating Pyruvate Dehydrogenase Activity▽†

Po-Chi Soo,[1]‡ Yu-Tze Horng,[1]‡ Meng-Jiun Lai,[3] Jun-Rong Wei,[1] Shang-Chen Hsieh,[1] Yung-Lin Chang,[1] Yu-Huan Tsai,[1] and Hsin-Chih Lai[1,2]*

Department of Clinical Laboratory Sciences and Medical Biotechnology, National Taiwan University College of Medicine, Taipei, Taiwan, Republic of China[1]; Department of Laboratory Medicine, National Taiwan University Hospital and National Taiwan University College of Medicine, Taipei, Taiwan, Republic of China[2]; and Department of Laboratory Medicine and Biotechnology, College of Medicine, Tzu Chi University, Hualien, Taiwan, Republic of China[3]

Received 18 May 2006/Accepted 28 August 2006

The protein pirin, which is involved in a variety of biological processes, is conserved from prokaryotic microorganisms, fungi, and plants to mammals. It acts as a transcriptional cofactor or an apoptosis-related protein in mammals and is involved in seed germination and seedling development in plants. In prokaryotes, while pirin is stress induced in cyanobacteria and may act as a quercetinase in *Escherichia coli*, the functions of pirin orthologs remain mostly uncharacterized. We show that the *Serratia marcescens* pirin (pirin$_{Sm}$) gene encodes an ortholog of pirin protein. Protein pull-down and bacterial two-hybrid assays followed by sodium dodecyl sulfate-polyacrylamide gel electrophoresis and electrospray ionization-tandem mass spectrometry analyses showed the pyruvate dehydrogenase (PDH) E1 subunit as a component interacting with the pirin$_{Sm}$ gene. Functional analyses showed that both PDH E1 subunit activity and PDH enzyme complex activity are inhibited by the pirin$_{Sm}$ gene in *S. marcescens* CH-1. The *S. marcescens* CH-1 pirin$_{Sm}$ gene was subsequently mutated by insertion-deletion homologous recombination. Accordingly, the PDH E1 and PDH enzyme complex activities and cellular ATP concentration increased up to 250%, 140%, and 220%, respectively, in the *S. marcescens* CH-1 pirin$_{Sm}$ mutant. Concomitantly, the cellular NADH/NAD$^+$ ratio increased in the pirin$_{Sm}$ mutant, indicating increased tricarboxylic acid (TCA) cycle activity. Our results show that the pirin$_{Sm}$ gene plays a regulatory role in the process of pyruvate catabolism to acetyl coenzyme A through interaction with the PDH E1 subunit and inhibiting PDH enzyme complex activity in *S. marcescens* CH-1, and they suggest that pirin$_{Sm}$ is an important protein involved in determining the direction of pyruvate metabolism towards either the TCA cycle or the fermentation pathways.

The protein pirin is widely found in mammals, plants, fungi, and also prokaryotic organisms (32). While the cellular functions of pirin show diversity and pirin homologs play important roles in a number of different biological processes, cellular localization of pirin is not restricted to specific compartments. In eukaryotes, pirin was initially isolated through a yeast two-hybrid screen from the HeLa cell cDNA library and is localized within cell nuclei; it acts as an interactor with nuclear factor I/CCAAT box transcription factor (32). In an attempt to identify downstream nuclear targets of Bcl-3 by using yeast two-hybrid screening of the expression cDNA library derived from human activated B cells, it was found that pirin interacts with and increases the DNA-binding activity of Bcl-3–p50 complex (Bcl-3 is a member of the IκB family that inhibits NF-κB activity) (6). A recent report from Orzaez et al. further showed that lepirin, a tomato homolog of human pirin, is involved in programmed cell death (21). On the other hand, in *Arabidopsis*, a pirin ortholog (AtPirin1) was isolated as a protein interacting with the α subunit of G protein through the yeast two-hybrid screen. AtPirin1 is involved in the regulation of seed germination and early seedling development of *Arabidopsis* (16). The human pirin crystalline structure was subsequently determined by Pang et al. (22), who showed that pirin comprises two β-barrel domains, with a potential Fe(II) cofactor bound within the cavity of the N-terminal domain. These findings suggest an enzymatic role for pirin, most likely in biological redox reactions involving oxygen (22).

In prokaryotes, *pirA*, encoding an ortholog of pirin, together with an adjacent gene, *pirB*, is up-regulated under high salinity and some other stress conditions in the cyanobacterium *Synechocystis* sp. strain PCC 6803 (13). However, induction of the *pirAB* genes is not related to programmed cell death, and disruption of *pirA* did not affect the cellular gene expression profile (13). Adams and Jia (1) determined the crystalline structure of the pirin homolog YhhW from *Escherichia coli*, in which the YhhW structure shows similarity to human pirin. Through active-site analysis, YhhW was further shown to act as a 2,3-dioxygenase that degrades the antioxidant quercetin to 2-protocatechuoylphloroglucinol, with concomitant release of CO as a by-product (1).

Previous studies on selection for precocious-swarming mu-

* Corresponding author. Mailing address: Department of Clinical Laboratory Sciences and Medical Biotechnology, National Taiwan University College of Medicine, No. 1 Chan-Der Street, Taipei 100, Taiwan, Republic of China. Phone: 886 2 2312 3456, ext. 6931. Fax: 886 2 2371 1574. E-mail: hclai@ha.mc.ntu.edu.tw.

† Supplemental material for this article may be found at http://jb.asm.org/.

‡ These two authors contributed equally to this work.

▽ Published ahead of print on 15 September 2006.

tants derived from *Serratia marcescens* CH-1 by transposon mutagenesis (15, 28) identified a mutant strain in which a pirin gene homolog was inserted by use of a mini-Tn*5* transposon (P.-C. Soo and H.-C. Lai, unpublished data). In comparison to human pirin, which is a 32-kDa protein consisting of 290 amino acids, and to *E. coli* pirin (YhhW), which is a 25.4-kDa protein with 231 amino acids, bioinformatic analyses identified a 312-amino-acid, 35-kDa pirin ortholog (pirin$_{Sm}$) in *S. marcescens* strain Db11 (Sanger Institute; http://www.sanger.ac.uk/cgi-bin/BLAST/submitblast/s_marcescens). Subsequently, a 5-kb pirin$_{Sm}$ gene locus was cloned and sequenced in *S. marcescens* strain CH-1. In this study, using protein pull-down and bacterial two-hybrid screening assays followed by protein identification by electrospray ionization-tandem mass spectrometry (ESI-MS/MS) analyses, we showed that the pirin ortholog in *S. marcescens* CH-1 interacts with the E1 subunit of pyruvate dehydrogenase (PDH) complex. PDH E1 is one of the three subunits (E1, pyruvate dehydrogenase; E2, dihydrolipoamide dehydrogenase transacetylase; and E3, lipoamide dehydrogenase) of the PDH multienzyme complex, which is an assemblage that plays a pivotal role in cellular carbohydrate metabolism, catalyzing the oxidative decarboxylation of pyruvate and the subsequent acetylation of coenzyme A (CoA) to form acetyl-CoA (5, 19). During the process of PDH enzyme complex reactions, PDH E1 is responsible for the first step of the multistep process and catalyzes pyruvate decarboxylation, followed by transferring the hydroxyethyl group to thiamine diphosphate (ThDP), which together with Mg^{2+} acts as the reaction cofactor (7). Subsequent gene deletion and biochemical analyses showed that pirin$_{Sm}$ regulated (inhibited) PDH E1 and PDH enzyme complex activities. In accordance, the cellular ATP concentration and NADH/NAD^+ ratio increased in the pirin$_{Sm}$ gene-deleted *S. marcescens* mutant grown to late logarithmic phase. These results show a new role of pirin$_{Sm}$ involving in the regulation of pyruvate catabolism to acetyl-CoA. This may subsequently affect cellular central carbohydrate metabolism to go towards the tricarboxylic acid (TCA) cycle or fermentation pathway.

MATERIALS AND METHODS

Bacterial strains, plasmids, primers, and culture conditions. *S. marcescens* CH-1 (28) is a clinical isolate routinely maintained at 37°C on Luria-Bertani (LB) plates. The chromosomal DNA sequence of *S. marcescens* Db11 was determined at the Sanger Institute (http://www.sanger.ac.uk/cgi-bin/BLAST/submitblast/s_marcescens). The bacterial strains, plasmids, and primers used in this study are described in Table 1.

Enzymes and chemicals. DNA restriction and modification enzymes were purchased from Roche (Mannheim, Germany). *Taq* polymerase and PCR-related products were obtained from either Perkin-Elmer (Boston, MA) or Takara Biomedicals (Shiga, Japan). Other laboratory-grade chemicals were purchased from Sigma Chemical Company (St. Louis, MO) or Merck (Schwabach, Germany).

Recombinant DNA techniques. Unless otherwise indicated, standard protocols were used for DNA/DNA hybridization, plasmid and chromosomal DNA preparation, transformation, electroporation, PCR, restriction digestion, agarose gel electrophoresis, DNA recovery from agarose gels, DNA ligation, and conjugation. Southern blotting analysis of chromosomal DNA was performed using nylon membranes (Hybond N^+; Amersham, Piscataway, NJ) and a DIG High Prime labeling kit (Roche) according to the recommendations of the manufacturer. PCR DNA amplicons were cloned using pCR 2.1 and the TA cloning kit (Invitrogen, Carlsbad, CA). DNA sequencing and analysis were performed using a Perkin-Elmer Autosequencer model 377 with a *Taq* DyeDeoxy terminator cycle sequencing kit (Applied Biosystems, Foster, CA). The DNA sequences of PCR products were confirmed by sequencing both strands from two or three independent reactions.

Cloning the pirin$_{Sm}$ gene locus in *S. marcescens* CH-1. The primers Db11-pir-F and Db11-pir-R (Table 1), designed from the *S. marcescens* Db11 pirin DNA sequence, were used to amplify a 924-bp partial pirin DNA fragment showing high nucleic acid sequence identity (99%) to the Db11 pirin gene from *S. marcescens* strain CH-1. This DNA fragment was subsequently labeled and used as a probe to clone the pirin$_{Sm}$ gene locus from *S. marcescens* CH-1. Conventional restriction digestions, Southern blot hybridizations, cloning, and sequencing identified a 5-kb DNA fragment containing the pirin$_{Sm}$ gene (Fig. 1).

Construction of *S. marcescens* CH-1 pirin$_{Sm}$ gene insertion-deletion mutant PC103. For construction of the pirin$_{Sm}$ gene mutant, a protocol was designed for specific insertion of a 2-kb streptomycin (Sm)-resistant Ω cassette, excised from pHP45Ω, into the pirin$_{Sm}$ gene in *S. marcescens* CH-1 (23, 28). Briefly, the 5′ region of the pirin$_{Sm}$ gene was amplified by PCR using primer pair Pirk1 and Pirk2, TA cloned into pCR 2.1 (Invitrogen), and excised as a SalI/HindIII fragment. A second PCR product encompassing the 3′ region of the pirin$_{Sm}$ gene was generated using primer pair Pirk3 and Pirk4, TA cloned into pCR 2.1 (Invitrogen), and excised as a HindIII/EcoRI fragment. The two DNA fragments together with the Ω cassette were ligated with the SalI/EcoRI-digested pUT-mini-Tn*5*-Km1 suicide vector (8) to form plasmid pUT-pirin$_{Sm}$::Sm.

For gene inactivation by homologous recombination, pUT-pirin$_{Sm}$::Sm was transferred from *E. coli* S17-1(λ pir) to *S. marcescens* CH-1 by conjugation (15). Transconjugants were spread on LB plates containing streptomycin (100 μg/ml) and tetracycline (13 μg/ml). Mutant candidates were screened by colony PCR. Southern blot hybridization using the pirin$_{Sm}$ gene as a probe was performed to confirm the mutant genotype in which a double-crossover event had occurred (data not shown). The resultant pirin$_{Sm}$ mutant strain was designated *S. marcescens* PC103.

Western blot analysis. The Western blot procedures were modified from those described by Sambrook et al. (24). In brief, bacterial cells harvested were washed once in phosphate-buffered saline (PBS) (pH 7.5) and resuspended in cell lysis buffer [20 mM piperazine-*N*,*N*′-bis(2-ethanesulfonic acid) (PIPES) (pH 7.2), 100 mM NaCl, 1 mM phenylmethylsulfonyl fluoride). Samples were left for 30 min on ice and centrifuged at 14,000 rpm for 30 min at 4°C. The spent supernatants were then concentrated and analyzed by 12.5% sodium dodecyl sulfate-polyacrylamide gel electrophoresis (SDS-PAGE). The separated proteins were transferred to a polyvinylidene difluoride membrane (Amersham) and incubated in blocking buffer (5% milk, 0.1% Tween 20) for 1 h. Further incubations with anti-His monoclonal antibody or anti-pirin$_{Sm}$ polyclonal antibodies were then performed in blocking buffer for 1 h at room temperature, followed by treatment with horseradish peroxidase-conjugated anti-rabbit second antibody for another 1 h before development and X-ray film exposure (28).

GST pull-down assay. The ProFound pull-down glutathione *S*-transferase (GST) protein-protein interaction kit (Pierce, Rockford, IL) was used for GST pull-down assay. Oversynthesis of GST fusion proteins was achieved by culturing *E. coli* DH5α cells containing recombinant plasmids pSC10 (GST-tagged pirin$_{Sm}$ fusion protein in pGEX) in 3 ml of LB broth medium to the mid-logarithmic phase at 37°C, followed by addition of IPTG (isopropyl-β-D-thiogalactopyranoside) at a final concentration of 0.5 mM for induction. After further culture for 3 h, cells were centrifuged and then suspended in 100 μl of lysis buffer (20 mM Tris-HCl (pH 8.0), 100 mM NaCl, 1 mM EDTA, 0.5% NP-40) containing leupeptin (1 μg/ml), pepstatin A (1 μg/ml), and phenylmethylsulfonyl fluoride (1 mM). Glutathione-Sepharose 4B beads (20 μl) (Amersham) were then added to the spent supernatant, and the mixture was incubated with mild shaking for 2 h at 4°C. Beads washed three times with PBS (pH 7.4)–1% Triton X-100 buffer were subsequently added to 500 μl of spent cell lysates of *S. marcescens* CH-1 or 0.5 mM IPTG-induced *E. coli* BL21(DE3)(pBG20). pBG20 is a recombinant plasmid containing His-tagged *S. marcescens* PDH E1 (AceE$_{Sm}$) fusion proteins. The reaction mixture was incubated at 4°C for 1 h to allow interaction between GST-pirin$_{Sm}$ and the His-tagged fusion proteins. Beads were subsequently washed with PBS (pH 7.4)–1% Triton X-100 buffer, and proteins were eluted with 10 mM glutathione before separation by 12.5% SDS-PAGE and detection by immunoblotting.

Bacterial two-hybrid screening. The bacterial two-hybrid system used in this study is based on interaction-mediated reconstitution of adenylate cyclase activity in an *E. coli* host (14). Briefly, interaction between T25-pirin$_{Sm}$ and PDH-E1-T18 fusion proteins leads to the cytoplasmic production and assembly of functional adenylate cyclase in *E. coli* DHM1. This was detected qualitatively by the ability of *E. coli* cells to ferment maltose on maltose-MacConkey agar plates (Difco, Franklin, NJ) to form red colonies (17). IPTG (0.5 mM) was included in the medium to induce full expression and synthesis of hybrid proteins when necessary.

TABLE 1. Bacterial strains, plasmids, and primers used in this study

Strain, plasmid, or primer	Relevant characteristics	Source or reference
Strains		
Serratia marcescens		
CH-1	Clinical isolate	28
PC103	CH-1 pirin$_{Sm}$::Sm, Sm^r	This study
Escherichia coli		
CC118(λ*pir*)	λ$^-$-*pir* lysogen of CC118 [Δ(*ara-leu*) *araD* Δ*lacX* 74 *galE galK phoA20 thi-1 rpsE rpoB argE*(Am) *recA1*]; permissive host for suicide plasmids requiring the Pir protein	23
S17-1(λ*pir*)	λ$^-$-*pir* lysogen of S17-1 [*thi pro hsdR hsdM*$^+$ *recA* RP4 2-Tc::Mu-Km::Tn*7* (Tp^r Sm^r)]; permissive host able to transfer suicide plasmids requiring the Pir protein by conjugation to recipient cells	23
BL21(DE3)	*E. coli* B F$^-$ *ompT hsdS* (r_B^- m_B^-) *dcm*$^+$ Tet^r *gal* (DE3) *endA* Hte	Stratagene
Plasmids		
pUT-Sm	Suicide plasmid requiring the Pir protein for replication and containing a mini-Tn*5* cassette containing Sm^r genes	23
pKT25	Encodes the T25 fragment of *B. pertussis* adenylate cyclase, corresponding to the first 224 amino acids of CyaA	14
pKT25-zip	Leucine zipper of GCN4 genetically fused in frame to the T25 fragment	14
pUT18	Encodes the T18 fragment (amino acids 225 to 399 of CyaA)	14
pUT18C-zip	Leucine zipper of GCN4 genetically fused in frame to the T18 fragment; pKT25-zip and pUT18C-zip serve as positive controls for complementation	14
pBAD18-Kan	Cloning and expression vector, arabinose regulation; Km^r	28
pGEX	Expression vector, GST Tag	Pharmacia Biotech
pSC10	pGEX::pirin$_{Sm}$; Amp^r	This study
pSC11	pGEX::*nlpB*$_{Sm}$; Amp^r	This study
pSC12	pGEX::*aceE*$_{Sm}$; Amp^r	This study
pSC15	pBAD18-Kan::pirin$_{Sm}$; Km^r	This study
pSC16	pUT-Sm derivative carrying pirin$_{Sm}$ gene inserted with Sm^r omega cassette; Sm^r	This study
pSC17	pKT25::pirin$_{Sm}$; Km^r	This study
pSC18	pUT18::*aceE*$_{Sm}$; Amp^r	This study
pSC19	pGEX::*aceF*$_{Sm}$; Amp^r	This study
pSC20	pGEX::*lpdA*$_{Sm}$; Amp^r	This study
pRSET	Expression vector, His Tag	Invitrogen
pBG20	pRSET::His-*aceE*$_{Sm}$; a 2.7-kb DNA fragment containing the PDH E1 gene (*aceE*$_{Sm}$) from *S. marcescens* CH-1 was PCR amplified and cloned into pRSET vector; Amp^r	This study
Primers		
Db11-pir-F	5′-ATGAGTCAGCCACGTCCT-3′	
Db11-pir-R	5′-GGCAGGCGTGGTGCGGTCA-3′	
Pirk-1	5′-GTCGACGGCCGGAGCGACCAAGT-3′	
Pirk-2	5′-AAGCTTAACACAGGACAGCTCCC-3′	
Pirk-3	5′-AAGCTTGCCATACCAAGGCTGA-3′	
Pirk-4	5′-GATATCGACATCTGACTAACGGAGC-3′	

Protein identification. In-gel digestion and mass spectrometric analysis were performed at EverNew Biotechnology, Inc. (Taipei, Taiwan), using procedures described previously (30, 34). Briefly, the gel piece was washed in 1 ml of 25 mM NH_4HCO_3 for 10 min and then in 1 ml of 25 mM NH_4HCO_3–50% acetonitrile for 10 min. After drying in a SpeedVac (ThermoSavant, Waltham, MA), the gel was incubated with 50 ml of 2% (vol/vol) β-mercaptoethanol in the dark for 20 min. Following incubation, an equal volume of 10% (vol/vol) vinylpyridine in 25 mM NH_4HCO_3–50% acetonitrile was added. After 20 min of incubation, the gel was washed several times in 1 ml of 25 mM NH_4HCO_3 and then dehydrated in 25 mM NH_4HCO_3 with 50% acetonitrile. The SpeedVac-dried gel was then treated with 50 ng of modified trypsin (Promega, Madison, WI) in an adequate volume of 25 mM NH_4HCO_3 at 37°C overnight. The resultant peptides were extracted with 200 μl of 0.1% formic acid, dried in the SpeedVac, and then stored at −20°C until further use.

Electrospray ionization-tandem mass spectrometry was performed using a ThermoFinnigan LCQ Deca ion trap mass spectrometer (Waltham, MA) interfaced with an Agilent 1100 high-pressure liquid chromatography (HPLC) system (Agilent Technologies, Palo Alto, CA). A 150- by 0.3-mm Agilent ZORBAX 300SB C_{18} column (3-μm particle diameter, 300-Å pore size) with mobile phases A (0.1% formic acid in water) and B (0.085% formic acid in acetonitrile) was used. The peptides were eluted at a flow rate of 5 μl/min, with gradients that consisted of 5% to 16% B over 5 min, 16% to 20% B over 40 min, and 20% to 65% B over 40 min.

The spectra for the eluates were acquired as successive sets of three scan modes, i.e., MS, zoom, and MS scans, as described previously (30, 34). The MS scan determined the intensity of the ions in the *m*/*z* range of 395 to 1605, and a specific ion was selected for the zoom and MS/MS scans. The former examined the charge number of the selected ion, and the latter acquired the spectrum (collision-induced dissociation [CID] spectrum or MS/MS spectrum) for the fragment ions derived by CID. In the first analysis, the most abundant ion in an MS spectrum was selected for the CID experiment; in the second analysis, only the ions with *m*/*z* values corresponding to the potential phosphopeptides were selected for the CID experiment. The acquired CID spectra were interpreted using TurboSequest software (ThermoFinnigan), which matched tandem mass spectra against a nonredundant protein database.

Synthesis and purification of *S. marcescens* PDH E1, E2, and E3 subunits. PDH subunits E1, E2, and E3 were overproduced in *E. coli* DH5α cells containing pSC12, pSC19, and pSC20, respectively. Briefly, overnight cultures of *E. coli* cells transformed with each recombinant plasmid were diluted 1:10 in fresh LB medium and grown for 2 h at 37°C before addition of 0.1 mM

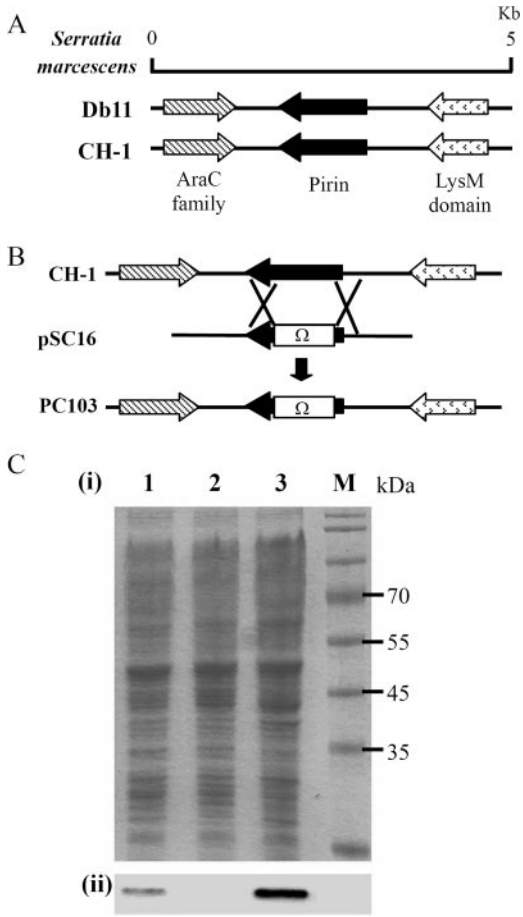

FIG. 1. Genetic map of the *S. marcescens* pirin gene locus and construction of the pirin$_{Sm}$ gene deletion mutant *S. marcescens* PC103. (A) Genetic maps of *S. marcescens* Db11 and CH-1 pirin gene loci. The LysM domain (2) and AraC family (29) are proteins encoded, respectively, by the two genes identified upstream and downstream of the pirin$_{Sm}$ gene. (B) Construction of the pirin$_{Sm}$ gene knockout mutant strain PC103 by insertion of a Sm resistance gene Ω cassette into the *S. marcescens* CH-1 pirin gene through homologous recombination (28). pSC16 is a recombinant suicide vector for insertion-deletion mutagenesis of the pirin$_{Sm}$ gene. (C) Western blot analysis of pirin$_{Sm}$ production. Panel i, whole-cell crude extracts were separated by 12.5% SDS-PAGE and subjected to Coomassie brilliant blue staining. Panel ii, results of pirin$_{Sm}$ detection using anti-pirin$_{Sm}$ polyclonal antibodies. Lane 1, *S. marcescens* CH-1; lane 2, *S. marcescens* PC103; lane 3, *S. marcescens* PC103 transformed with pSC15(pBAD18-Kan::pirin$_{Sm}$); lane M, protein marker.

IPTG. After another 3 h of growth, cells were centrifuged and resuspended in lysis buffer (20 mM Tris-HCl [pH 8.0], 100 mM NaCl, 1 mM EDTA, 1% TritonX-100). Cells were lysed by sonication followed by centrifugation at 10,000 × *g* for 20 min at 4°C. The supernatant was then subjected to glutathione-Sepharose purification (26).

PDH E1 and PDH enzyme complex activity assays. Determination of PDH E1 was achieved by an assay that measures the rate of reduction of the artificial electron acceptor 2,6-dichlorophenolindophenol (DCPIP) by the E1 component, with pyruvate as a substrate (DCPIP assay) (12). The decrease in absorbance at 600 nm was monitored at 30°C in a suspension comprising 0.2 mM ThDP, 2 mM $MgCl_2$, 50 μM DCPIP, 100 mM potassium phosphate (pH 7.0), and spent crude protein extracts (20 to 50 μg), purified E1 protein, or other protein reactants at of 15 μg each. After incubation at 30°C for 10 min, reactions were initiated by addition of pyruvate (final concentration of 400 μM), followed by monitoring the amount of DCPIP reduced over the reaction period of up to 2 h. DCPIP reduction was calculated by the absorbance change, using a molar absorption constant of ε_{600} = 11,000 M^{-1} cm^{-1} for DCPIP (35).

PDH enzyme complex catalytic activity was measured using the PDH assay (5). The PDH assay measured the rate of NADH formation by absorbance at 340 nm at 30°C (5, 10). The reaction was started by addition of final concentrations of 2 mM pyruvate and 0.13 mM CoA to an assay mixture containing 0.2 mM ThDP, 1 mM $MgCl_2$, 2.6 mM cysteine HCl, 2.5 mM NAD^+, 50 mM potassium phosphate (pH 7.0), and 20 to 50 μg of the reconstituted PDH enzyme complex (E1/E2/E3 molar ratio = 2:2:1) or spent crude cellular extracts. Specific activities were expressed as units (micromoles of NADH formed per minute) per milligram of whole-cell lysate in the assay.

Determination of acetyl-CoA concentration. Procedures for determination of acetyl-CoA concentrations followed the protocols of Deutsch et al. (9). Briefly, acetyl-CoA was separated by HPLC using a C_{18} column (Mightysil RP-18 GP; Kanto Chemical Co., Tokyo, Japan) and eluted with an interrupted linear gradient of acetonitrile in 0.1 mol/liter potassium phosphate (pH 5.0). Initial conditions were 81% solvent A (0.1 mol/liter potassium phosphate, pH 5.0) and 19% solvent B (40% acetonitrile in solvent A); a constant flow rate of 0.25 ml/min was used during separation. The column was equilibrated at 3% of B for 10 min between injections. Detection was by absorbance at a wavelength of 254 nm. Retention times of the acetyl-CoA standards were used to identify the peaks on the HPLC chromatograms of each reaction sample. To see the effect of pirin$_{Sm}$ on production of acetyl-CoA, the reaction samples, which contained 0.2 mM ThDP, 1 mM $MgCl_2$, 2.6 mM cysteine HCl, 2 mM pyruvate, 0.13 mM CoA, 2.5 mM NAD^+, 50 mM potassium phosphate (pH 7.0), and crude cellular extracts containing 50 μg of protein, were incubated for 1 h at 30°C. Each sample was then applied to HPLC for quantification of acetyl-CoA concentration by peak height with reference to standards of known acetyl-CoA concentrations.

Cellular ATP concentration assay. The BacTiter-Glo microbial assay kit (Promega) together with a photon-counting Autolumat luminometer LB953 (Berthold, Dortmund, Germany) for detection of light emission were used for determination of cellular ATP concentration. Briefly, spent cell lysates (100 μl) prepared from fixed amounts of bacteria (volume [milliliters] × optical density at 600 nm [OD_{600}] = 0.8) were mixed thoroughly with 100 μl of substrate solution. This was followed by incubation for 2 min at room temperature. The luminescence was then measured at 5-min intervals, and light emission was recorded for 10 seconds. Results were obtained in triplicate as ATP concentrations obtained after calculation against a standard curve at time intervals of 10 min.

Measurement of NAD^+ and NADH concentrations. Dinucleotide extraction was modified from previously described methods (27). Equal numbers of bacterial cells (determined by volume [milliliters] × OD_{600} = 5) were harvested at 5 h postinoculation in the late log phase by centrifugation for 15 min at 2,500 × *g*. After washing of the bacterial pellet in PBS, either 1 ml of 0.2 M HCl (NAD^+ extraction) or 1 ml of 0.2 M KOH (NADH extraction) was added. Samples were boiled for 10 min. After centrifugation (5 min, 10,000 × *g*, 4°C), cell-free lysates were neutralized. Dinucleotide levels were measured with an enzymatic cycling assay described by Bernofsky and Swan (3). Briefly, 400 μl of cycling buffer [2.2 ml of 623 mM bicin, 2.2 ml of 2.6 mM 3-(4,5-dimethyl-thiazoyl-2)-2,5-diphenyltetrazolium bromide (MTT), 2.2 ml of 26 mM EDTA, 1.75 ml of 10.4 mM phenazine ethosulfate, and 0.4 ml ethanol] were added to 400 μl of neutralized extraction solution. After incubation for 5 min at room temperature in the dark, the reaction was initiated by adding 160 μl of 1.3-mg/ml yeast alcohol dehydrogenase (Sigma), and the rate of MTT reduction was monitored spectrophotometrically at 570 nm. The intracellular concentrations of dinucleotides were determined by known concentrations of NAD^+ and NADH (0, 2.5, 5, 25, and 50 μM). All assays were performed in triplicate from three independent cultures.

Determination of acetate concentration. The amount of acetate was determined as previously described (31). Briefly, equal numbers of bacterial cells (determined by volume [milliliters] × OD_{600} = 5) were centrifuged for 15 min at 2,500 × *g*. The bacterial pellets were suspended in PBS before incubation at 80°C for 15 min to stop the enzymatic reactions. The cell lysates were centrifuged for 5 min at 10,000 × *g* at 4°C, and acetate concentrations in the supernatants were determined using a kit purchased from R-Biopharm (Marshall, MI).

RESULTS

A pirin ortholog in *S. marcescens*. During the process of selecting for *S. marcescens* precocious-swarming mutants by transposon mutagenesis assay (15), a pirin gene homolog in a mutant strain was identified to be interrupted by the transposon (Soo and Lai, unpublished data). The pirin gene in *S.*

marcescens CH-1 was subjected to genetic and functional analyses. Through conventional restriction, cloning, and sequencing analyses, a 5-kb DNA fragment containing a putative pirin$_{Sm}$ gene was identified in *S. marcescens* CH-1 (GenBank accession number DQ288954). Genetic maps flanking the pirin$_{Sm}$ gene were similar for CH-1 and Db11 (Fig. 1A). Upstream of the pirin$_{Sm}$ gene was an open reading frame predicted to encode a LysM protein domain (2), and downstream of the pirin$_{Sm}$ gene was an open reading frame encoding an AraC family protein (29) (Fig. 1A).

Extensive computational searches using programs such as NCBI-BLAST and FASTA were performed to identify the *S. marcescens* pirin-like proteins from the data banks. *S. marcescens* pirin homologs are highly conserved, from many bacterial species to human pirin (26% identity). Pirin orthologs identified in bacteria include those from *Pseudomonas aeruginosa* PA14 (54% identity), an *Acinetobacter* sp. (49% identity), *Corynebacterium glutamicum* (43% identity), *Brucella melitensis* (37% identity), *E. coli* (YhhW protein, 37% identity), *Ralstonia solanacearum* (31% identity), *Agrobacterium tumefaciens* (27% identity), and *Clostridium perfringens* (24% identity). The amino acid sequence alignments of *S. marcescens* CH-1 pirin$_{Sm}$ with these pirin orthologs are shown in Fig. S1 in the supplemental material. Based on the results of protein sequence pattern analysis from the MOTIFS (http://motif.genome.jp/) and SMART (http://smart.embl-heidelberg.de/) programs, the *S. marcescens* pirin protein displays a typical bicupin fold comprising a single N-terminal metal coordination site (pirin domain) and a C-terminal pirin-C conserved domain.

Interaction of *S. marcescens* pirin with the PDH E1 subunit. Current data cannot directly indicate the function of pirin$_{Sm}$ in *S. marcescens*. To characterize pirin$_{Sm}$ function, the potential proteins interacting with pirin$_{Sm}$ in *S. marcescens* CH-1 were targeted. A recombinant plasmid, pSC10, in which the pirin$_{Sm}$ gene was N-terminally fused with GST to form a GST-pirin$_{Sm}$ fusion protein was constructed. pSC10 was subsequently transformed into *E. coli* DH5α for oversynthesis of the GST-pirin$_{Sm}$ protein. After purification, GST protein pull-down assay was performed. Separation of captured proteins by SDS-PAGE highlighted three major bands with predicted molecular masses of 99 kDa (band a), 76 kDa (band b), and 50 kDa (band c) after comparison with the negative controls (GST-*nlpB*$_{Sm}$ [28] fusion and GST protein only) (Fig. 2).

Amino acid sequence analyses using ESI-MS/MS were subsequently performed for protein identification. Comparison of the partial amino acid sequences of each protein with nonredundant protein databases in the SEQUEST Browser (http://fields.scripps.edu/sequest/) highlighted three proteins with the highest identity to the respective bands. They were *E. coli* PDH subunit E1 (band a), *E. coli* PDH subunit E2 (band b), and *E. coli* 2-oxoglutarate dehydrogenase (ODH) complex subunit E2 (band c) (see Fig. S2 in the supplemental material). PDH E1 was subsequently selected for further study.

The GST pull-down assay was further performed to see whether oversynthesized PDH E1 protein subunit interacted with oversynthesized pirin$_{Sm}$. A recombinant plasmid, pBG20, encoding a His-tagged PDH E1$_{Sm}$ (AceE$_{Sm}$) fusion protein was constructed. The pBG20 and pSC10 plasmids were transformed into *E. coli* BL21(DE3) and *E. coli* DH5α, respectively, followed by induction with 0.5 mM IPTG for protein oversynthesis. The spent supernatants of whole-cell lysates prepared from both cell types at a volume ratio of 1:1 were mixed thoroughly and incubated at 4°C for 2 h before addition of glutathione-Sepharose 4B beads for capturing protein complexes. SDS-PAGE followed by Western blot analysis using anti His-Tag antibody confirmed that the *S. marcescens* PDH E1 subunit was pulled down by GST-pirin$_{Sm}$ (Fig. 3A).

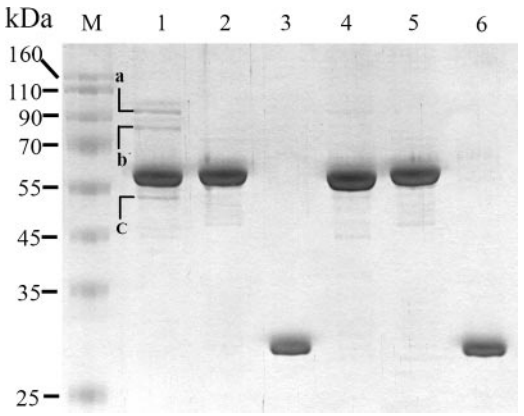

FIG. 2. Use of protein pull-down assay for identification of *S. marcescens* proteins interacting with pirin$_{Sm}$. Glutathione-Sepharose 4B beads were used to capture protein complexes comprising GST-pirin$_{Sm}$ fusion protein and the potential pirin$_{Sm}$ interactors in CH-1. After elution, SDS-PAGE analysis was performed for protein separation. The cell lysate of *E. coli* DH5α containing either pSC10 (GST-pirin$_{Sm}$ fusion protein was oversynthesized) (lane 1), pSC11 (GST-NlpB$_{Sm}$ [28] fusion protein was oversynthesized) (lane 2), or pGEX (GST Tag only) (lane 3) was mixed with CH-1 lysate at a volume ratio of 1:1. Lane 4, GST-pirin$_{Sm}$ fusion protein; lane 5, GST-NlpB$_{Sm}$ fusion protein; lane 6, GST Tag protein; lane M, protein markers. Identification of the separated proteins was achieved by amino acid sequence analysis using electrospray ionization-MS/MS and comparison of the partial amino acid sequences with nonredundant protein databases in the SEQUEST Browser (http://fields.scripps.edu/sequest/). The three proteins with highest identity scores were *E. coli* PDH subunit E1 (band a, 99 kDa), *E. coli* PDH subunit E2 (band b, 76 kDa), and *E. coli* succinate dehydrogenase subunit E2 (band c, 50 kDa).

Oversynthesized PDH E1 was subsequently used as the bait to confirm its interaction with pirin$_{Sm}$ in *S. marcescens* CH-1. The recombinant plasmid pSC12 encoding the GST-PDH E1$_{Sm}$ fusion protein was transformed into *S. marcescens* CH-1, followed by 0.5 mM IPTG induction and pull-down assay to see whether pirin$_{Sm}$ was captured. SDS-PAGE analysis followed by Western blot analysis using monospecific polyclonal anti-pirin$_{Sm}$ antibody confirmed pirin$_{Sm}$ as the interactor with PDH E1 (Fig. 3B).

To confirm the interaction between pirin$_{Sm}$ and PDH E1, a bacterial two-hybrid assay was further performed. A change of colony color from colorless to pink-red after transforming both pSC17 (plasmid pKT25 [14] containing the pirin$_{Sm}$ gene) and pSC18 (plasmid pUT18 [14] containing the PDH E1 *aceE*$_{Sm}$ gene) into *E. coli* DHM1 indicated specific activation of maltose catabolic genes (Fig. 3C), thus confirming a positive interaction between these two proteins. In brief, the PDH E1 subunit interacted with *S. marcescens* pirin.

Inhibition of PDH E1 activity by pirin$_{Sm}$. To see whether the PDH E1 activity was affected by oversynthesis of pirin$_{Sm}$, the DCPIP assay (12) was performed. Spent cell lysates of *E. coli*

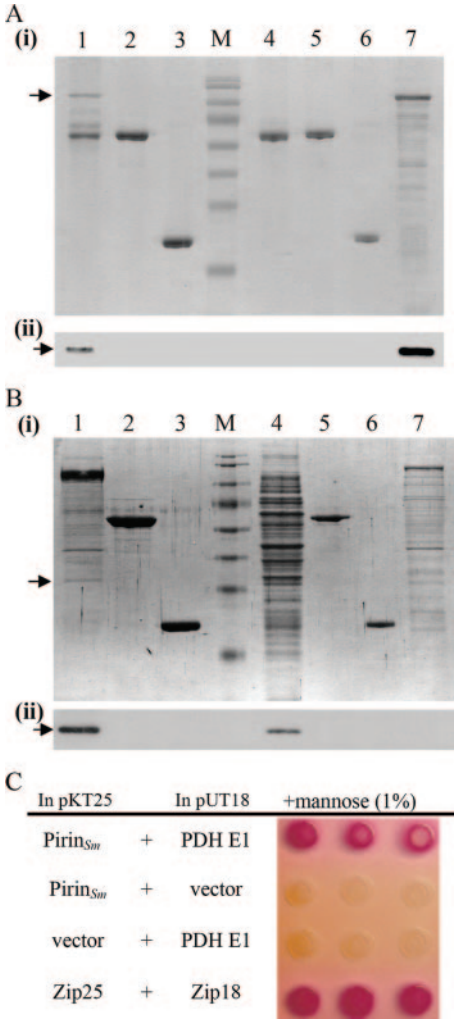

FIG. 3. Confirmation of interaction between *S. marcescens* pirin and PDH E1. (A) In vitro GST pull-down assay followed by SDS-PAGE (panel i) and Western blot analysis (panel ii) using anti-His-Tag antibody was performed to confirm the interaction between GST-pirin$_{Sm}$ and His-PDH E1. GST-pirin$_{Sm}$ and His-PDH E1 were oversynthesized in *E. coli* before the assay. Lane 1, GST-pirin$_{Sm}$ with His-PDH E1; lane 2, GST-NlpB$_{Sm}$ with His-PDH E1; lane 3, GST Tag with His-PDH E1; lane 4, GST-pirin$_{Sm}$ only; lane 5, GST-NlpB$_{Sm}$ only; lane 6, GST Tag only; lane 7, *E. coli*(pBG20) spent crude extract containing His-PDH E1; arrow, His-PDH E1; lane M, protein markers (same as those in Fig. 2). (B) Oversynthesized GST-PDH E1 was used as the bait to confirm its interaction with pirin$_{Sm}$. After interaction, SDS-PAGE (panel i) and Western blot analysis using anti-pirin$_{Sm}$ polyclonal antibody (panel ii) were performed. Lane 1, GST-PDH E1 with CH-1 lysate; lane 2, GST-NlpB$_{Sm}$ with CH-1 lysate; lane 3, GST Tag with CH-1 lysate; lane 4, spent CH-1 cell lysate; lane 5, GST-NlpB$_{Sm}$ only; lane 6, GST Tag protein only; lane 7, spent crude extract containing GST-PDH E1 from *E. coli* DH5α; arrow, pirin$_{Sm}$. (C) Bacterial two-hybrid assay. Colony color changed from colorless to pink-red after transformation of both pSC17 (pKT25 plasmid containing the pirin$_{Sm}$ gene) and pSC18 (pUT18 plasmid containing the PDH E1 *aceE*$_{Sm}$ gene) into *E. coli* DHM1, indicating specific activation of maltose catabolic genes and interaction between GST-pirin$_{Sm}$ and His-PDH E1 (14). Zip25 and Zip18 were used as positive controls.

BL21(DE3) cells containing either pBG20 (PDH E1 subunit), pSC10 (pirin$_{Sm}$), or the pGEX vector were prepared after cells were grown to late logarithmic phase at an OD_{600} of 0.6 under induction with 0.5 mM IPTG. Measurements of PDH E1 activities were achieved by mixing both cell lysates (25 μg PDH E1 lysate with 50 μg GST-pirin$_{Sm}$ or GST Tag lysate) with externally added pyruvate at a final concentration of 400 μM as the substrate. As shown in Fig. 4A, the PDH E1 activities of mixed cell lysates from *E. coli* BL21(DE3)(pSC10) and *E. coli* BL21(DE3)(pBG20) were 30% lower than those from *E. coli* BL21(DE3)(pGEX) and *E. coli* BL21(DE3)(pBG20).

Inhibition of PDH E1 activity in *S. marcescens* CH-1 by pirin$_{Sm}$ gene overexpression. As *S. marcescens* CH-1(pSC15) (pirin$_{Sm}$ gene expression under the control of the pBAD promoter) cells were grown to an OD_{600} of 0.6 in LB broth culture, the amount of pirin$_{Sm}$ protein was induced up to fivefold in the presence of 0.02% arabinose (data not shown), and the PDH E1 activity was reduced up to 40% compared with that from *S. marcescens* CH-1(pBAD18) (Fig. 4B).

We reasoned that the PDH E1 activity might be increased in the *S. marcescens* CH-1 pirin$_{Sm}$ mutant strain. To evaluate this possibility, the pirin$_{Sm}$ gene was knocked out by insertion-deletion homologous recombination through an Sm resistance Ω cassette (23) in *S. marcescens* CH-1 to form the mutant strain *S. marcescens* PC103 (Fig. 1B). Southern blot hybridization (data not shown) and Western blot analysis (Fig. 1C) confirmed deletion of the pirin$_{Sm}$ gene in *S. marcescens* CH-1. No significant difference in growth dynamics in LB broth cultures was observed between CH-1 and PC103 (data not shown). Spent cellular crude extracts of CH-1 and PC103 cells grown to an OD_{600} of 0.6 were prepared and used in the DCPIP assay. PDH E1 activity in PC103 cells was 250% higher than that in CH-1 cells (Fig. 4C). Complementation of *S. marcescens* PC103 by transforming pSC15 into *S. marcescens* PC103 cells inhibited the PDH E1 activity (Fig. 4D), while transforming the control vector pBAD18 into *S. marcescens* PC103 cells did not. Thus, *S. marcescens* PDH E1 activity was inhibited by pirin$_{Sm}$.

To characterize the specific inhibition of PDH E1 activity by pirin$_{Sm}$, GST-tagged PDH E1 and GST-tagged pirin$_{Sm}$ were purified from *E. coli* DH5α(pSC12) and *E. coli* DH5α(pSC10), respectively (Fig. 4E). The DCPIP assay showed that GST-PDH E1 activity was 30% lower in the presence of GST-pirin$_{Sm}$ than that of GST alone or GST-NlpB$_{Sm}$ fusion protein (28) (Fig. 4F).

Pirin$_{Sm}$ inhibition of PDH enzyme complex activity in *S. marcescens*. Inhibition of PDH E1 activity by pirin$_{Sm}$ strongly suggested that PDH enzyme complex activity would be inhibited. To confirm this supposition, a total of 50 μg of spent cellular crude extract each was prepared from *S. marcescens* CH-1 and PC103 and was used in the PDH activity assay. The cellular PDH activity in *S. marcescens* PC103 cells was 40% higher than that in *S. marcescens* CH-1 (Fig. 4G). On the other hand, oversynthesis of pirin$_{Sm}$ in the *S. marcescens* PC103 mutant strain led to inhibition of PDH activity by 30% compared with *S. marcescens* PC103 containing the control vector (Fig. 4H). To rule out possible background interferences, the in vitro-reconstituted PDH enzyme complex comprising E1, E2, and E3 at a molecular ratio of 2:2:1 was further used for measurement of PDH activity. As shown in Fig. 4I, the reconstituted PDH activity was inhibited about 35% by GST-pirin$_{Sm}$ compared with the GST-NlpB$_{Sm}$ and GST-alone controls.

Increased PDH activity in the pirin$_{Sm}$ gene-deleted mutant strain *S. marcescens* PC103 should result in increased acetyl-

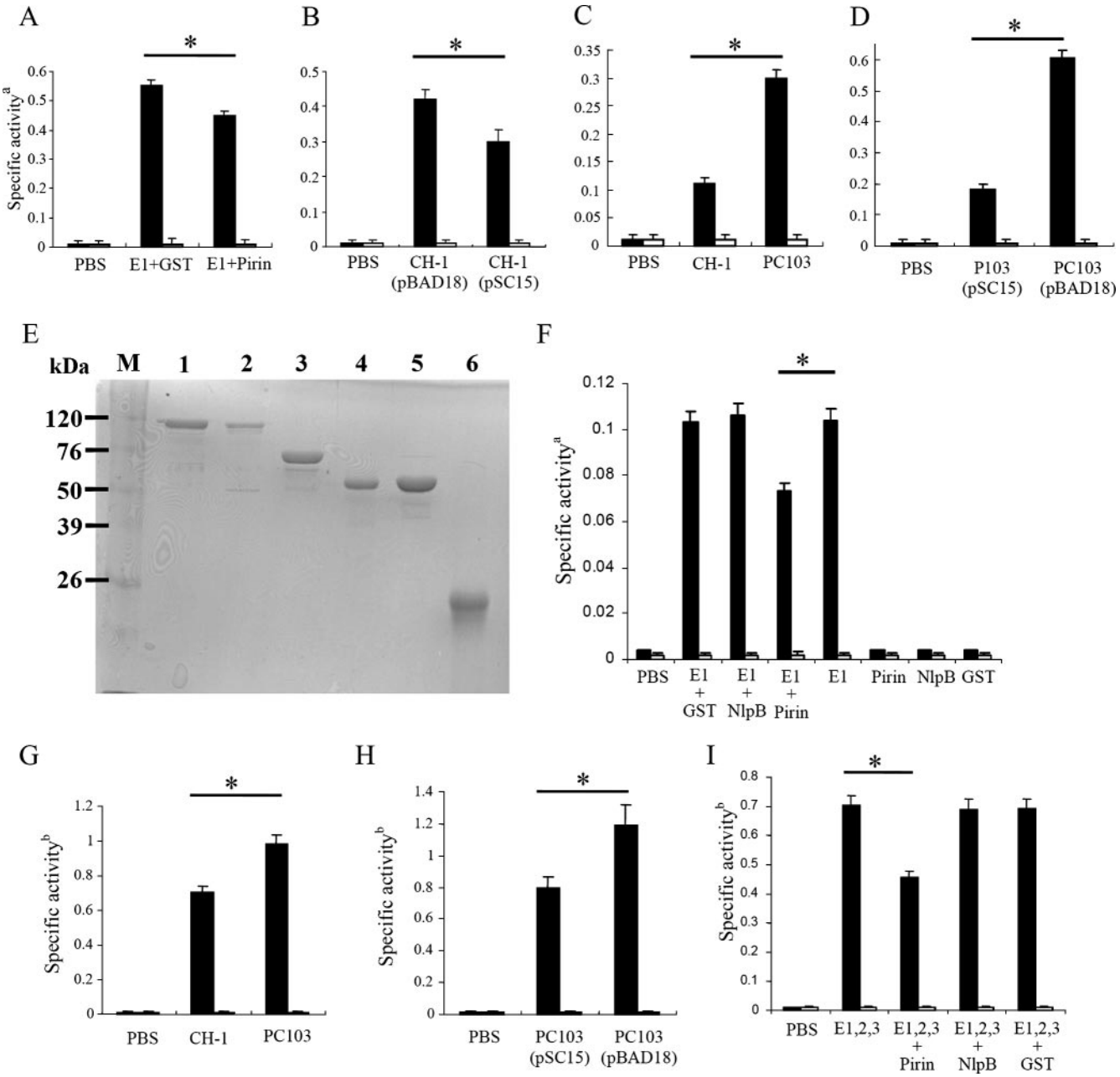

FIG. 4. Pirin$_{Sm}$ inhibits PDH E1 and PDH enzyme complex activities. (A) Effect of pirin$_{Sm}$ on PDH E1$_{Sm}$ specific activity. *E. coli* BL21(DE3) was used as the host for protein synthesis. (B) Effect of pirin$_{Sm}$ gene overexpression (0.02% arabinose induction) from pSC15 on PDH E1$_{Sm}$ specific activity in *S. marcescens* CH-1. (C) Effect of pirin$_{Sm}$ gene deletion on PDH E1$_{Sm}$ specific activity in *S. marcescens* CH-1. (D) Effect of pirin$_{Sm}$ gene overexpression (0.02% arabinose induction) from pSC15 on PDH E1$_{Sm}$ specific activity in *S. marcescens* PC103. (E) Purification of *S. marcescens* PDH E1, E2, and E3 subunits in *E. coli* DH5α cells. Lane 1, GST-E1 subunit (pSC12); lane 2, GST-E2 subunit (pSC19); lane 3, GST-E3 subunit (pSC20); lane 4, GST-pirin (pSC10); lane 5, GST-NlpB$_{Sm}$ (pSC11); 6, GST protein (pGEX vector). (F) Effect of purified pirin$_{Sm}$, NlpB$_{Sm}$, and GST (15 μg each) on specific activity of purified PDH E1 subunit (15 μg). (G) PDH enzyme complex activity in *S. marcescens* CH-1 and PC103. (H) Effect of pirin$_{Sm}$ gene overexpression (0.02% arabinose induction) from pSC15 on specific PDH enzyme complex activity in *S. marcescens* PC103. (I) Effect of pirin$_{Sm}$ on reconstituted PDH enzyme complex at an E1/E2/E3 molar ratio of 2:2:1. The DCPIP assay (12) was used to measure PDH E1 activity; the rate of NADH formation was measured spectrophotometrically at a wavelength of 340 nm (5) to measure PDH enzyme complex activity. Black and white bars indicate reactions with or without pyruvate added as the substrate. PBS (pH 7.4) was used as the negative control for all assays. CH-1, *S. marcescens* CH-1; PC103, a pirin$_{Sm}$ gene insertion-deletion mutant strain derived from *S. marcescens* CH-1; pBAD18, pBAD18-Kan control vector; pSC15, pBAD18-Kan::pirin$_{Sm}$ gene; NlpB$_{Sm}$, a membrane lipoprotein identified in *S. marcescens* CH-1 (28). a, change in OD_{600} per minute per milligram of protein. b, change in OD_{340} per minute per milligram of protein. Values are means and standard deviations from three independent experiments. ∗, $P < 0.05$.

TABLE 2. PDH enzyme complex activities and acetyl-CoA concentrations in *S. marcescens* CH-1 and PC103 cells

Bacterial strain	PDH enzyme complex activity		Acetyl-CoA concn	
	μmol NADH formed/mg/min (mean ± SD)[a]	%	nmol/mg protein (mean ± SD)[a]	%
CH-1	0.701 ± 0.035	100	0.750 ± 0.055	100
PC103	0.983 ± 0.053	140	1.125 ± 0.087	150
PC103(pBAD18)	1.189 ± 0.134	170	1.165 ± 0.076	155
PC103(pSC15)	0.794 ± 0.071	113	0.706 ± 0.042	94

[a] Data are from three independent experiments.

CoA production. To evaluate this supposition, spent cellular crude extracts of *S. marcescens* CH-1 and PC103 were prepared, followed by C_{18} reverse-phase HPLC separation for determination of acetyl-CoA concentrations. The acetyl-CoA concentration increased about 50% in *S. marcescens* PC103 in comparison to that in *S. marcescens* CH-1 (Table 2). Complementation of the pirin$_{Sm}$ gene in *S. marcescens* PC103 by transformation of pSC15 into *S. marcescens* PC103 cells reduced the acetyl-CoA concentration up to 40% compared with that of *S. marcescens* PC103 (Table 2). Thus, pirin$_{Sm}$ inhibited PDH enzyme complex activity in *S. marcescens* CH-1.

Cellular ATP concentration and NADH/NAD$^+$ ratio are increased in *S. marcescens* PC103. Following the process of converting pyruvate into acetyl-CoA by the PDH enzyme complex, acetyl-CoA is further oxidized through TCA cycle intermediates, accompanied by synthesis of NADH and reduced flavin adenine dinucleotide ($FADH_2$) (4). The majority of the cellular ATP is produced from these reduced NADH and $FADH_2$ compounds after further respiration reactions (25). Alternatively, acetyl-CoA is converted to acetate through dissimilation via the PTA-ACKA (phosphotransacetylaseacetate kinase) pathway and produces less ATP (33). Thus, alteration of the acetyl-CoA concentration should result in a change in cellular ATP concentration. Indeed, the cellular ATP concentration in *S. marcescens* PC103 grown to an OD_{600} of 0.6 in the late log phase was increased 220% compared with that in *S. marcescens* CH-1 (Fig. 5A); complementation of *S. marcescens* PC103 with pSC15 reduced the ATP concentration to the normal level (Fig. 5B). The increase in ATP concentration in *S. marcescens* PC103 might have been due to activation of either the TCA cycle or the PTA-ACKA pathway or both. To clarify this, the NADH/NAD$^+$ ratio, which shows TCA cycle activity and intracellular redox status (31), and cellular acetate concentration were determined. While there was no significant difference in acetate concentration (Fig. 5C), the NADH/NAD$^+$ ratio in *S. marcescens* PC103 was significantly higher than that in *S. marcescens* CH-1 (0.759 versus 0.439; $P < 0.05$) (Fig. 5D), suggesting that increased TCA cycle activity is mainly responsible for increased ATP concentration in *S. marcescens* PC103.

DISCUSSION

Very few studies on characterization of pirin orthologs in prokaryotes have been reported. Thus, whether pirin$_{Sm}$ functions as an enzyme, a regulator involved in any signaling pathway, or a protein enhancing the interaction between DNA and protein complexes remains to be further characterized among bacterial species. The *S. marcescens* pirin shows sequential and structural similarity to *E. coli* YhhW (20); however, whether pirin$_{Sm}$ is secreted outside the *S. marcescens* cells and degrades quercetin remains to be determined. In this report, through protein-protein interaction, genetic, and biochemical analyses, our results showed that pirin$_{Sm}$ binds with PDH E1 and inhibits its PDH E1 and PDH enzyme complex activities. Although PDH E1, PDH E2, and ODH E2 were identified as pirin$_{Sm}$ interactor proteins, we still could not rule out the possibility that the PDH E3 subunit was also among the interacting components, as PDH E3 might be dissociated from E1 and E2 during the purification process. At the same time, the intrigu-

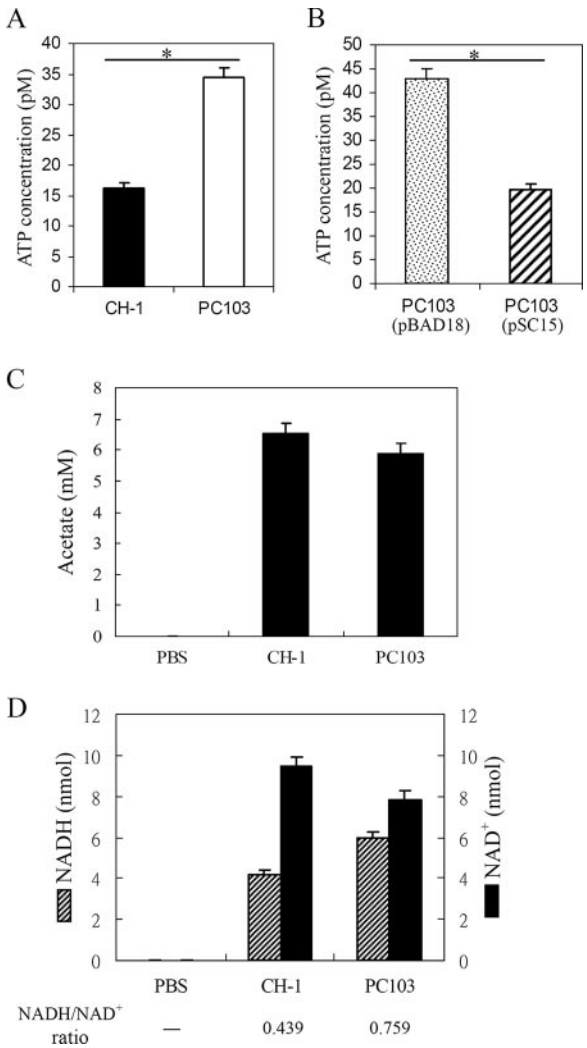

FIG. 5. Cellular ATP concentration and NADH/NAD$^+$ ratio are increased in the pirin$_{Sm}$ gene deletion mutant strain *S. marcescens* PC103. Bacterial cells were grown to an OD_{600} of 0.6, followed by determination of cellular ATP concentration (A and B), cellular acetate concentration (C), and intracellular redox status through measuring the concentrations and determining the ratio of NADH to NAD$^+$ (D). CH-1, *S. marcescens* wild-type strain; PC103, pirin gene deletion mutant *S. marcescens* strain; PC103(pBAD18) and PC103(pSC15), *S. marcescens* PC103 containing the pBAD18-Kan control vector or pBAD18-Kan::pirin$_{Sm}$, respectively. All results are means and standard deviations from three independent experiments. *, $P < 0.05$.

ing phenomenon that the estimated molecular mass of the interactor protein PDH E2 was 76 kDa after SDS-PAGE analysis was observed (Fig. 2, lane 1, band b). This is different from the predicted molecular mass of PDH E2 in *E. coli* (see Fig. S2 in the supplemental material) and *S. marcescens* CH-1, which is 66 kDa. One of the explanations is that posttranslational modification of PDH E2 might occur in *S. marcescens* CH-1. Furthermore, besides PDH E1 and E2, ODH E2 was also identified. ODH E2 is involved in the process of converting α-ketoglutarate to succinate-CoA and releasing CO_2 and NADH, which is one of the enzymatic reactions belonging to the TCA cycle (4, 25). The composition of the ODH enzyme complex shows similarity to that of the PDH enzyme complex, as both complexes comprise E1, E2, and E3 subunits and functionally are components of the biochemical pathway leading to generation of NADH and $FADH_2$ for subsequent ATP generation. Thus, interaction of pirin$_{Sm}$ with components of these proteins strongly indicates that pirin$_{Sm}$ is involved in the process of determination of cellular ATP concentration and energy production. Due to the significant increase in NADH/NAD^+ ratio but not cellular acetate concentration in the pirin$_{Sm}$ mutant (Fig. 5C and D), the effect of increased ATP concentration should be attributed mostly to increased TCA cycle activity. Comparatively, the PTA-ACKA pathway, which also produces ATP, seemed not to play a dominant role in the process.

On the basis of both sequential and structural similarities, pirin orthologs are classified as a subfamily of the cupin superfamily (11, 32). The cupin superfamily is one of the most functionally diverse protein classes and includes both enzymatic and nonenzymatic members, ranging from isomerases and epimerases that are involved in the modification of cell wall carbohydrates to nonenzymatic storage proteins in plant seeds and transcriptional cofactors in humans (11). Prediction of the secondary and tertiary structures of pirin$_{Sm}$ through use of the JOY program (18) showed that the structure of pirin$_{Sm}$ is similar to that of human pirin (Soo and Lai, unpublished data). These two proteins are predicted to contain a conserved N-terminal metal-binding domain and a C-terminal β-barrel domain, and they show three conserved histidine residues (His^{77}, His^{79}, and His^{121} for pirin$_{Sm}$; His^{56}, His^{58}, and His^{101} for human pirin) and a conserved glutamate residue (Glu^{123} for pirin$_{Sm}$; Glu^{103} for human pirin) in the N-terminal motifs (see Fig. S1 in the supplemental material), suggesting a functional conservation between the two proteins. However, differences are still evident, including the amino acids surrounding the predicted metal ion-binding site (data not shown). Thus, the conformation of pirin proteins might vary under different environments. This might explain the phenomenon that pirin family orthologs interact with different proteins and affect diverse biological processes.

How pirin$_{Sm}$ interacts with and regulates PDH E1 and subsequently PDH enzyme complex activity remains undetermined. What we understand currently is that a compact pirin$_{Sm}$ is essential for interaction with PDH E1, as no protein-protein interaction reaction was observed when we dissected the pirin$_{Sm}$ protein into N-terminal and C-terminal domains (data not shown). Further deletion and functional analyses combined with surface plasmon resonance protein-protein interaction analysis should help us understand more about the pirin$_{Sm}$-PDH E1 interaction mechanism. As PDH is responsible for conversion of pyruvate into acetyl-CoA, increased PDH enzyme complex activity should mean that the direction of cellular pyruvate metabolism shunts towards the TCA cycle and subsequently the electron transport chain so that more cellular ATP is produced by oxidative phosphorylation through this aerobic respiratory pathway (25). This usually occurs when cells are growing aerobically or at the logarithmic phase in LB broth culture. In contrast, a reduction in PDH enzyme complex activity suggests that pyruvate metabolism is diverted towards the fermentation pathways, whereby less ATP is produced (25). This frequently occurs when cells are grown under anaerobic conditions or are growing into the stationary phase. While deletion of the pirin$_{Sm}$ gene in *S. marcescens* CH-1 led to increased total cellular ATP production even though cells were grown to the early stationary phase at high cell density, the pirin$_{Sm}$ concentration increased as cells grew into the transitional phase, and it peaked at the stationary phase (Soo and Lai, unpublished data). Together these results suggest that pirin$_{Sm}$ might regulate *S. marcescens* central carbohydrate metabolism through diverting the reactions towards the fermentation pathways (thus producing less ATP and accumulating more fermentation products) as cells are grown to a high density. It is predicted that the ferrous ion Fe(II) is located within the N-terminal metal-binding motif of human pirin (22). If it is the same for pirin$_{Sm}$, then pirin$_{Sm}$ might be involved in sensing the redox status (NADH/NAD^+ ratio) within the cell through oxidation or reduction of ferrous ion. Such sensing might then affect pirin$_{Sm}$ conformation and the subsequent interaction with and modulation of PDH enzyme complex activity. To confirm this, determination of the three-dimensional protein-protein interaction structure between pirin$_{Sm}$ and PDH E1 by X-ray crystallography will have to be performed.

ACKNOWLEDGMENTS

This work was supported by grants from the National Science Council (NSC-94-2320-B-002-078 and NSC-95-2320-B-002-061) and the Aim for Top University Program Excellence Research Projects 2006, National Taiwan University.

REFERENCES

1. **Adams, M. A., and Z. Jia.** 2005. Structural and biochemical evidence for an enzymatic quinone redox cycle in *Escherichia coli*: identification of a novel quinol monooxygenase. J. Biol. Chem. **280:**8358–8363.
2. **Bateman, A., and M. Bycroft.** 2000. The structure of a LysM domain from E. coli membrane-bound lytic murein transglycosylase D (MltD). J. Mol. Biol. **299:**1113–1119.
3. **Bernofsky, C., and M. Swan.** 1973. An improved cycling assay for nicotinamide adenine dinucleotide. Anal. Biochem. **53:**452–458.
4. **Buchanan, B. B., and D. I. Arnon.** 1990. A reverse KREBS cycle in photosynthesis: consensus at last. Photosynth. Res. **24:**47–53.
5. **Danson, M. J., A. R. Fersht, and R. N. Perham.** 1978. Rapid intramolecular coupling of active sites in the pyruvate dehydrogenase complex of Escherichia coli: mechanism for rate enhancement in a multimeric structure. Proc. Natl. Acad. Sci. USA **75:**5386–5390.
6. **Dechend, R., F. Hirano, K. Lehmann, V. Heissmeyer, S. Ansieau, F. G. Wulczyn, C. Scheidereit, and A. Leutz.** 1999. The Bcl-3 oncoprotein acts as a bridging factor between NF-kappaB/Rel and nuclear co-regulators. Oncogene **18:**3316–3323.
7. **de Kok, A., A. F. Hengeveld, A. Martin, and A. H. Westphal.** 1998. The pyruvate dehydrogenase multi-enzyme complex from Gram-negative bacteria. Biochim. Biophys. Acta **1385:**353–366.
8. **de Lorenzo, V., M. Herrero, U. Jakubzik, and K. N. Timmis.** 1990. Mini-Tn5 transposon derivatives for insertion mutagenesis, promoter probing, and chromosomal insertion of cloned DNA in gram-negative eubacteria. J. Bacteriol. **172:**6568–6572.
9. **Deutsch, J., S. I. Rapoport, and T. A. Rosenberger.** 2002. Coenzyme A and

short-chain acyl-CoA species in control and ischemic rat brain. Neurochem. Res. **27:**1577–1582.
10. **Domingo, G. J., H. J. Chauhan, I. A. Lessard, C. Fuller, and R. N. Perham.** 1999. Self-assembly and catalytic activity of the pyruvate dehydrogenase multienzyme complex from *Bacillus stearothermophilus*. Eur. J. Biochem. **266:**1136–1146.
11. **Dunwell, J. M., A. Culham, C. E. Carter, C. R. Sosa-Aguirre, and P. W. Goodenough.** 2001. Evolution of functional diversity in the cupin superfamily. Trends Biochem. Sci. **26:**740–746.
12. **Fries, M., H. I. Jung, and R. N. Perham.** 2003. Reaction mechanism of the heterotetrameric (alpha2beta2) E1 component of 2-oxo acid dehydrogenase multienzyme complexes. Biochemistry **42:**6996–7002.
13. **Hihara, Y., M. Muramatsu, K. Nakamura, and K. Sonoike.** 2004. A cyanobacterial gene encoding an ortholog of Pirin is induced under stress conditions. FEBS Lett. **574:**101–105.
14. **Jobling, M. G., and R. K. Holmes.** 2000. Identification of motifs in cholera toxin A1 polypeptide that are required for its interaction with human ADP-ribosylation factor 6 in a bacterial two-hybrid system. Proc. Natl. Acad. Sci. USA **97:**14662–14667.
15. **Lai, H. C., P. C. Soo, J. R. Wei, W. C. Yi, S. J. Liaw, Y. T. Horng, S. M. Lin, S. W. Ho, S. Swift, and P. Williams.** 2005. The RssAB two-component signal transduction system in *Serratia marcescens* regulates swarming motility and cell envelope architecture in response to exogenous saturated fatty acids. J. Bacteriol. **187:**3407–3414.
16. **Lapik, Y. R., and L. S. Kaufman.** 2003. The Arabidopsis cupin domain protein AtPirin1 interacts with the G protein alpha-subunit GPA1 and regulates seed germination and early seedling development. Plant Cell **15:**1578–1590.
17. **Miller, J. H.** 1992. A short course in bacterial genetics. Cold Spring Harbor Laboratory Press, Cold Spring Harbor, NY.
18. **Mizuguchi, K., C. M. Deane, T. L. Blundell, M. S. Johnson, and J. P. Overington.** 1998. JOY: protein sequence-structure representation and analysis. Bioinformatics **14:**617–623.
19. **Neidhardt, F. C.** 1996. Respiration, p. 151–169. *In* F. C. Neidhardt, R. Curtiss III, J. L. Ingraham, E. C. C. Lin, K. B. Low, B. Magasanik, W. S. Reznikoff, M. Riley, M. Schaechter, and H. E. Umbarger (ed.), *Escherichia coli* and *Salmonella*: cellular and molecular biology. American Society for Microbiology, Washington, DC.
20. **Oka, T., and F. J. Simpson.** 1971. Quercetinase, a dioxygenase containing copper. Biochem. Biophys. Res. Commun. **43:**1–5.
21. **Orzaez, D., A. J. de Jong, and E. J. Woltering.** 2001. A tomato homologue of the human protein PIRIN is induced during programmed cell death. Plant Mol. Biol. **46:**459–468.
22. **Pang, H., M. Bartlam, Q. Zeng, H. Miyatake, T. Hisano, K. Miki, L. L. Wong, G. F. Gao, and Z. Rao.** 2004. Crystal structure of human pirin: an iron-binding nuclear protein and transcription cofactor. J. Biol. Chem. **279:**1491–1498.
23. **Prentki, P., and H. M. Krisch.** 1984. In vitro insertional mutagenesis with a selectable DNA fragment. Gene **29:**303–313.
24. **Sambrook, J., E. F. Fritsch, and T. Maniatis.** 1989. Molecular cloning: a laboratory manual, 2nd ed. Cold Spring Harbor Laboratory Press, Cold Spring Harbor, NY.
25. **Schagger, H.** 2002. Respiratory chain supercomplexes of mitochondria and bacteria. Biochim. Biophys. Acta **1555:**154–159.
26. **Smith, D. B., and K. S. Johnson.** 1988. Single-step purification of polypeptides expressed in *Escherichia coli* as fusions with glutathione S-transferase. Gene **67:**31–40.
27. **Snoep, J. L., M. J. Teixeira de Mattos, P. W. Postma, and O. M. Neijssel.** 1990. Involvement of pyruvate dehydrogenase in product formation in pyruvate-limited anaerobic chemostat cultures of *Enterococcus faecalis* NCTC 775. Arch. Microbiol. **154:**50–55.
28. **Soo, P. C., J. R. Wei, Y. T. Horng, S. C. Hsieh, S. W. Ho, and H. C. Lai.** 2005. Characterization of the *dapA-nlpB* genetic locus involved in regulation of swarming motility, cell envelope architecture, hemolysin production, and cell attachment ability in *Serratia marcescens*. Infect. Immun. **73:**6075–6084.
29. **Tobes, R., and J. L. Ramos.** 2002. AraC-XylS database: a family of positive transcriptional regulators in bacteria. Nucleic Acids Res. **30:**318–321.
30. **Tsay, Y. G., Y. H. Wang, C. M. Chiu, B. J. Shen, and S. C. Lee.** 2000. A strategy for identification and quantitation of phosphopeptides by liquid chromatography/tandem mass spectrometry. Anal. Biochem. **287:**55–64.
31. **Vuong, C., J. B. Kidder, E. R. Jacobson, M. Otto, R. A. Proctor, and G. A. Somerville.** 2005. *Staphylococcus epidermidis* polysaccharide intercellular adhesin production significantly increases during tricarboxylic acid cycle stress. J. Bacteriol. **187:**2967–2973.
32. **Wendler, W. M., E. Kremmer, R. Forster, and E. L. Winnacker.** 1997. Identification of pirin, a novel highly conserved nuclear protein. J. Biol. Chem. **272:**8482–8489.
33. **Wolfe, A. J.** 2005. The acetate switch. Microbiol. Mol. Biol. Rev. **69:**12–50.
34. **Yang, C. C., C. H. Huang, C. Y. Li, Y. G. Tsay, S. C. Lee, and C. W. Chen.** 2002. The terminal proteins of linear Streptomyces chromosomes and plasmids: a novel class of replication priming proteins. Mol. Microbiol. **43:**297–305.
35. **Zahn, J. A., D. J. Bergmann, J. M. Boyd, R. C. Kunz, and A. A. DiSpirito.** 2001. Membrane-associated quinoprotein formaldehyde dehydrogenase from *Methylococcus capsulatus* Bath. J. Bacteriol. **183:**6832–6840.